Journal of Molecular Graphics and Modelling 50 (2014) 1–9

Contents lists available at ScienceDirect

Journal of Molecular Graphics and Modelling

journal homepage: www.elsevier.com/locate/JMGM

In silico investigation of medicinal spectrum of imidazo-azines from the perspective of multitarget screening against malaria, tuberculosis and Chagas disease

Manoj Kumar, Barnita Makhal, Vinod Kumar Gupta, Anuj Sharma*

Med. Chem. Lab, Department of Chemistry, Indian Institute of Technology Roorkee, Roorkee, Uttarakhand 247 667, India

ARTICLE INFO

Article history:
Received 22 June 2013
Received in revised form 14 February 2014
Accepted 21 February 2014
Available online 12 March 2014

Keywords:
Docking
Imidazo-azines
Ligand efficiency
Multitarget screening
Lead-likeness

ABSTRACT

A chemical database of 30 representative imidazo-azines was built and screened against important tropical disease targets by computational docking. After three rounds of screening, an interaction profile was generated and analyzed. On the basis of binding energy and ligand efficiency, it was concluded that in general, imidazo-azine scaffold has a potential of being selective and simultaneous inhibitor against the five receptors *Pf*-dihydrofolate reductase, *Pf*-enoyl acyl carrier protein reductase, *Pf*-protein kinase 7, *Mt*-pantothenate synthetase and *Mt*-thymidine monophosphate kinase. Interestingly, two compounds 2-(4-chlorophenyl)-*N*-cyclohexyl-6-methyl*H*-imidazo[1,2-*a*]pyridine-3-amine (MCL011) and *N*-cyclohexyl-2-(4-methoxyphenyl)-6-methyl*H*-imidazo[1,2-*a*]pyridine-3-amine (MCL017) showed highest binding energy against four targets *namely Pf*-dihydrofolate reductase, *Pf*-enoyl acyl carrier protein reductase, *Pf*-protein kinase 7 and *Mt*-pantothenate synthetase. Eventually, in order to improve the decision making and success rate in actual efficacy evaluations other criteria such as lead-likeness were envisaged.

1. Introduction

Reported as "global burden" malaria, tuberculosis and Chagas disease are amongst the major contributors to mortality and morbidity in most of the tropic and subtropics [1]. Chagas disease has been recognized as a neglected tropical disease (NTD) by WHO while malaria and tuberculosis are placed in "the big three diseases" along with AIDS [1]. These devastating diseases alone claim millions of death annually.

The current antimalarial arsenal relies on quinolines, antifolates and related substructures but because of the genesis and spread of the resistant malarial strain, most of the drugs except artemisinin have lost their effectiveness [2]. Likewise, isoniazids and related drugs like rifampicin, pyrazinamide, ethambutol, *etc.* form the mainstay of tuberculosis treatment. However, the emergence of extreme drug resistant (XDR), multi-drug resistant (MDR) and total drug resistant (TDR) forms of pathogen has seriously compromised the clinical utility of the current therapy [3]. Moreover, co-infection of HIV with tuberculosis and/or malaria has worsened the situation further. Chagas disease is usually treated by benznidazole (a nitroimidazole derivative) or nifurtimox (a nitrofuran derivative, Nfx). However, this therapy suffers from severe side effects and poor clinical efficacy [4]. The prevailing danger of drug-resistance and severe limitations of current chemotherapies has created a large gap between demand and supply of effective therapeutics. In order to bridge this gap effectively and timely; it is important to find newer and more effective molecules continuously.

In this context, we decided to investigate the medicinal spectrum of imidazo-azines against some important therapeutical targets from the perspective of computational multitarget screening. There were primarily three reasons for selection of amino-azines: (i) a wide range of therapeutic activities exhibited by this class of heterocycles like analgesic [5], anti-inflammatory [5], anti-proliferative [6], allosteric modulator of $GABA_A$ receptor [7], anti-viral [8], anti-bacterial and anti-microbial [9]. This scaffold is represented by marketed drugs such as zolimidine (an antiulcer drug), zolpidem (a hypnotic drug), alpidem (a non sedative anxiolytic), olprinone, and divaplon (Fig. 1); (ii) secondly, easy accessibility of N-fused bicyclic imidazo-azines through Groebke-Blackburn-Bienymé multi component reactions [10]; (iii) last but not the least, our ongoing interest in the synthesis of this class [11] and an understanding that these heterocycles have not been explored for the titled disease targets, especially at the molecular level.

* Corresponding author. Tel.: +91 13 3228 4751; fax: +91 13 3227 3560.
E-mail address: anujsharma.mcl@gmail.com (A. Sharma).

http://dx.doi.org/10.1016/j.jmgm.2014.02.006
1093-3263/

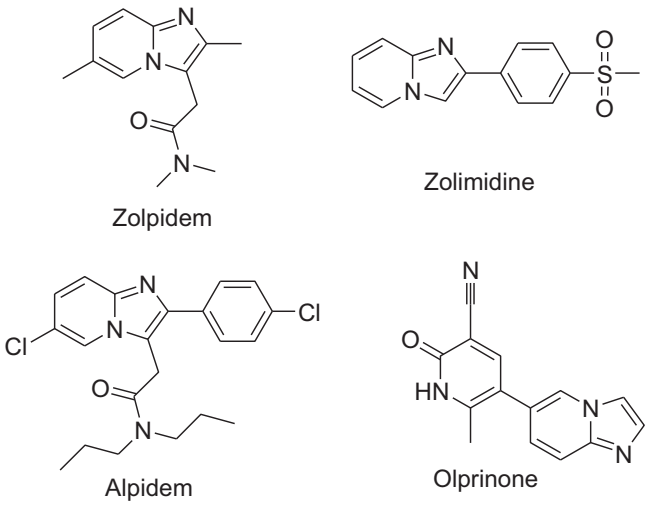

Fig. 1. Marketed drug having N-fused bicyclic imidazo-azines scaffold.

Above-mentioned multitarget screening is a relatively newer paradigm of drug discovery ventures. The aim of this approach is to identify a "key compound or scaffold" that can favorably interact with more than one receptor. The basic benefit of this screening is that inhibitor resistance can be greatly overcome by the decreased probability of simultaneous mutations of all the target proteins [13].

To achieve this aim, we selected a group of 10 well-validated drug targets from literature. The selection of targets was based on their biological role, selectivity and previous docking history.

The details of these targets are given below:

Malaria

Pf-dihydrofolate Reductase (DHFR) catalyzes the conversion of dihyrofolate to tetrahydrofolate that get converted into 5,10-methylenetetrahydrofolate which is necessary to provide a methyl group for the conversion of dUMP to dTMP in DNA synthesis pathway [12]. *Pf*-enoyl acyl carrier protein reductase (Enoyl ACP Reductase) catalyzes the reduction of *trans*-2 enoyl bond of enoyl-Acetyl CoA phosphate substrates of the malarial FAS II cycle [14]. *Pf*-protein kinase 7 (PK 7) can autophosphorylate as well as phosphorylate myelin basic protein and to a lesser extent, histone H2A as well as β-casein ultimately leading to the cell growth and proliferation [15].

Tuberculosis

Mt-shikimate kinase (SK) catalyzes the phosphorylation of shikimate to shikimate-3-phosphate, the fifth step of the shikimate pathway, leading to the biosynthesis of aromatic amino acids in pathogen [16]. *Mt*-pantothenate synthetase (PS) forms the amide bond formation between D-pantoate and β-alanine to form pantothenate (Vitamin B_5); required for the biosynthesis of Coenzyme A (CoA) and acyl carrier protein (ACP) which is necessary for many intracellular processes including fatty acid metabolism, cell signaling, synthesis of polyketides and non-ribosomal peptides [17]. *Mt*-thymidine monophosphate kinase (TMPK) promotes the conversion of deoxythymidine monophosphate (dTMP) to deoxythymidine diphosphate (dTDP) using ATP as a phosphoryl donor of the thymidine metabolism leading to the DNA synthesis [18]. *Mt*-MurE ligase preferentially adds meso-diaminopimelic acid (m-DAP) to the g-carboxyl groupof glutamic acid in uridine-5′-diphosphate-N-acetylmuramoyl-L-Alanine-D-Glutamate (UDPMurNAc-L-Ala-D-Glu) in peptidoglycan biosynthesis of the bacterial cell wall [19].

Chagas disease

Tc-trypanothione reductase (TR) reduces trypanothione disulfide (TS_2) to trypanothione dithiol [$T(SH)_2$] which scavenges the harmful oxygen species (ROS) such as superoxide anions (O_2), hydrogen peroxide (H_2O_2) and hydroxyl radicals (OH) formed as by-products of aerobic respiration in the parasite [20]. *Tc*-glyceraldehydes-3-phosphate dehydrogenase (G3PD) dehydrogenates glyceraldehyde-3-phosphate to 1,3-biphosphoglycerate, the sixth step of the glycolysis pathway [21]. The trypanosomal parasite *Trypanosoma cruzi* can evade host immune system. The parasite membrane-associated protein, *trans*-sialidase (TS), catalyzes the transfer of sialic acid molecules from host cell-surface glycoconjugates to its own surface mucin like glycoprotein, a very important step of its invasion stage [22].

Materials and methods

Ligand preparation

ChemDraw (Cambridgesoft Inc.) [23] was solely used for ligand preparation. 2D structure of the ligands (Table 1) were initially drawn which were converted into 3D. These 3D structures were then energy minimized and geometrically optimized (using AM1 force field).

Protein preparation

The X-ray crystal structures of wild type (WT) forms of *Pf*-DHFR–TS (1J3I.pdb) [24], *Pf*-Enoyl ACP Reductase (1NHG.pdb) [25], *Pf*-PK7 (2PMN.pdb) [15], *Mt*-SK (2DFN.pdb) [26], *Mt*-PS (1N2H.pdb) [27], *Mt*-TMPK (1G3U.pdb) [28], *Mt*-MurE ligase (2WTZ.pdb) [29], *Tc*-TR (1BZL.pdb) [20], *Tc*-G3PD (1QXS.pdb) [30] and *Tc*-TS (1S0I.pdb) [31] were used in this study. These structures contain the third-generation inhibitor WRA 609A, the inhibitor triclosan TCL 500A, the ATP-site inhibitor K51 344X, the substrate SKM 500A, the intermediate PAJ 1001A, the substrate TMP 217A, the substrate UAG 1498B, the substrates GCG 603A, S70 804A and SLT 923A respectively. Polar hydrogens were added and Gasteiger charges were computed in ADT. These structures were cleaned by removing crystallographic water, bound substrates and co-factors.

Docking Tool-AutoDock

AutoDock 4.2 (http://autodock.scripps.edu) [32] was employed for pose prediction and binding energy evaluation [33]. The default search function of AutoDock 4.2 is Lamarckian genetic algorithm (LGA), a hybrid of genetic algorithm and local search algorithm. The software accepts the ligand as well as the macromolecule coordinates as inputs and then seeks the help of LGA to generate the ligand positions and minimize binding energies using pre-calculated pair wise potential grid maps.

Grid parameter setting and docking calculation

Grids of suitable sizes (refer to supplementary information, Table S2) with default spacing were built and centered on the active site of the proteins under investigation with all the ligand atom types. Besides, an electrostatic and desolvation map was calculated. The parameters used in the docking study are mentioned below:

Table 1
Structural diversity of imidazo-azines used in the study.

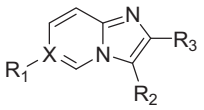

MCL001	R_1 = H, X = C, R_2 = $(CH_3)_3$CNH, R_3 = C_6H_5	MCL016	R_1 = H, X = C, R_2 = C_6H_{11}NH, R_3 = C_6H_4OMe
MCL002	R_1 = CH_3, X = C, R_2 = $(CH_3)_3$ CNH, R_3 = C_6H_5	MCL017	R_1 = CH_3, X = C, R_2 = C_6H_{11}NH, R_3 = C_6H_4OMe
MCL003	X = N, R_2 = $(CH_3)_3$ CNH, R_3 = C_6H_5	MCL018	X = N, R_2 = C_6H_{11}NH, R_3 = C_6H_4OMe
MCL004	R_1 = H, X = C, R_2 = C_6H_{11}NH, R_3 = C_6H_5	MCL019	R_1 = H, X = C, R_2 = $(CH_3)_3$ CNH, R_3 = H
MCL005	R_1 = CH_3, X = C, R_2 = C_6H_{11}NH, R_3 = C_6H_5	MCL020	R_1 = CH_3, X = C, R_2 = $(CH_3)_3$ CNH, R_3 = H
MCL006	X = N, R_2 = C_6H_{11}NH, R_3 = C_6H_5	MCL021	X = N, R_2 = $(CH_3)_3$ CNH, R_3 = H
MCL007	R_1 = H, X = C, R_2 = $(CH_3)_3$CNH, R_3 = C_6H_4Cl	MCL022	R_1 = H, X = C, R_2 = C_6H_{11}NH, R_3 = H
MCL008	R_1 = CH_3, X = C, R_2 = $(CH_3)_3$ CNH, R_3 = C_6H_4Cl	MCL023	R_1 = CH_3, X = C, R_2 = C_6H_{11}NH, R_3 = H
MCL009	X = N, R_2 = $(CH_3)_3$CNH, R_3 = C_6H_4Cl	MCL024	X = N, R_2 = C_6H_{11}NH, R_3 = H
MCL010	R_1 = H, X = C, R_2 = C_6H_{11}NH, R_3 = C_6H_4Cl	MCL025	R_1 = H, X = C, R_2 = $(CH_3)_3$ CNH, R_3 = C_4H_3O
MCL011	R_1 = CH_3, X = C, R_2 = C_6H_{11}NH, R_3 = C_6H_4Cl	MCL026	R_1 = CH_3, X = C, R_2 = $(CH_3)_3$ CNH, R_3 = C_4H_3O
MCL012	X = N, R_2 = C_6H_{11}NH, R_3 = C_6H_4Cl	MCL027	X = N, R_2 = $(CH_3)_3$ CNH, R_3 = C_4H_3O
MCL013	R_1 = H, X = C, R_2 = $(CH_3)_3$CNH, R_3 = C_6H_4OMe	MCL028	R_1 = H, X = C, R_2 = C_6H_{11}NH, R_3 = C_4H_3O
MCL014	R_1 = CH_3, X = C, R_2 = $(CH_3)_3$CNH, R_3 = C_6H_4OMe	MCL029	R_1 = CH_3, X = C,R_2 = C_6H_{11}NH, R_3 = C_4H_3O
MCL015	X = N, R_2 = $(CH_3)_3$CNH, R_3 = C_6H_4OMe	MCL030	X = N, R_2 = C_6H_{11}NH, R_3 = C_4H_3O

($(CH_3)_3$CNH = *tert*-Butylamino group, C_6H_{11}NH = Cyclohexylamino, C_6H_5 = Phenyl, C_6H_4Cl = Chlorophenyl, C_6H_4OMe = methoxyphenyl, C_4H_3O = furfuryl.

No. of final conformation (ga_run) 25;
Maximum no. of evaluations (ga_num_evals) 2500000;
Maximum no. of generations (ga_num_generation) 27000;
Mutation rate (ga_mutation_rate) 0.02;
Crossover rate (ga_crossover_rate) 0.8;
Local search on an individual in the population (ls_search_frequency) 0.06;
No. of top individuals to survive to next generation (ga_elitism) 1;
Maximum no. of iterations per local search (sw_max_its) 300;

The docking results were clustered on the basis of root mean square deviation (rmsd) and were ranked on the basis of free energy of binding.

Result and discussion

Analysis of the docking results is always a challenging task because it is tricky and subjective. It requires a fine tuning between two conflicting demands *i.e.* search for a global minima and computation within a reasonable span of time. To meet these requirements our docking engine; AutoDock combines two methods – rapid grid based energy evaluation & efficient search of torsional freedom [34]. Although AutoDock is time-tested and well-validated; but like any other computational tool it does not always guarantee best results due to inaccuracies of the scoring function. Other factors such as consideration of ligand flexibility, parameter setting, cluster pattern, visual inspection of the final result are also crucial for the success of a docking program [35–37]. Hence, instead of traditional approach of hit selection based solely on potency, a more holistic approach was employed here that included several additional aspects of lead discovery such as ligand efficiency and data driven assessment of ligand likeness. The main advantage of this approach was to identify lead like hits with minimum numbers of liabilities. In this light, following filters were used in the overall investigation.

A. Control docking/Redocking experiments and flexibility + Cluster analysis for benchmark: to validate our docking tool and to judge the credibility of the results.
B. Filter based on ligand efficiency/scoring function: to classify hits and non-hits.
C. Implementation of additional parameters such as lead-likeness: to improve the success rate in actual efficacy assays.

This methodology of exercising three tier filter mechanism in our study as succinctly describe in Scheme 1 is elaborated as below:

Control docking (Redocking) experiments and flexibility + cluster analysis for positive controls

Since the success rate of *in silico* studies, relies on the choice of screening tool, hence validation of the docking tools is a routine exercise. For this, all the co-crystallized substrates were removed

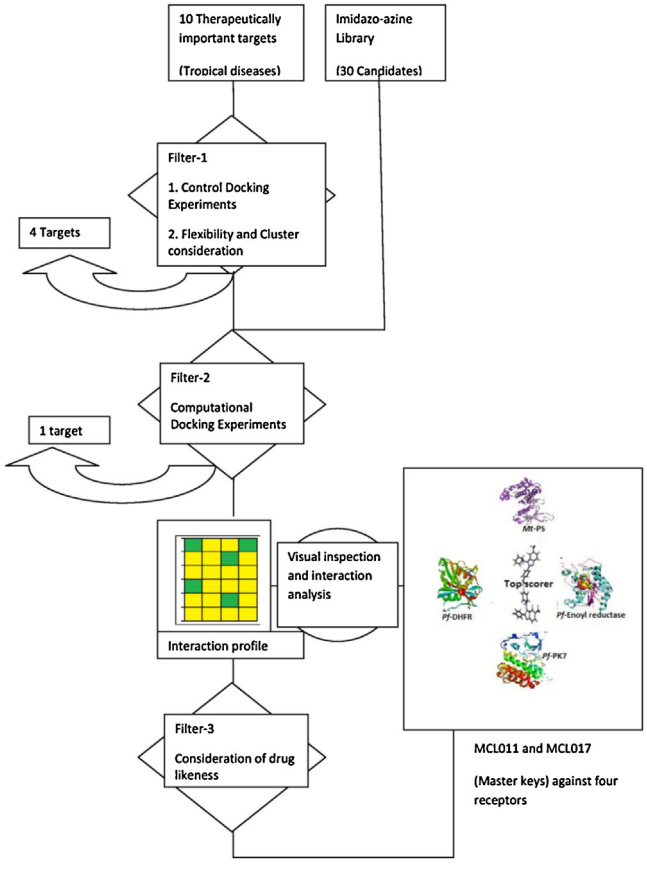

Scheme 1. Detail of the strategy used in multitarget screening of imidazo-azine library.

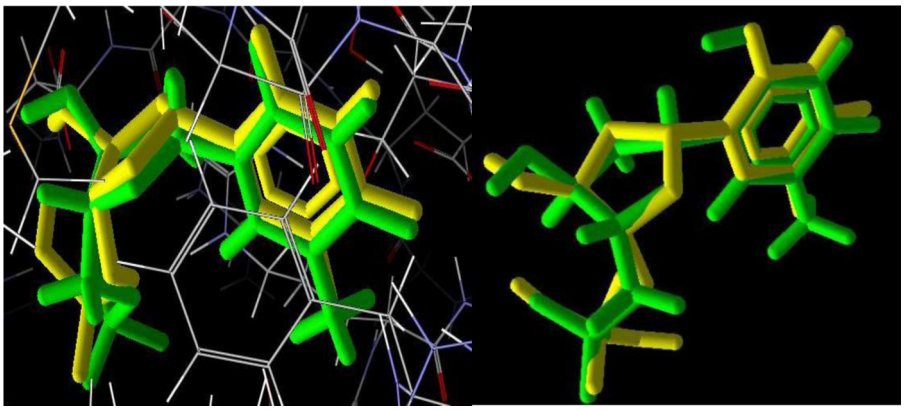

Fig. 2. Superimposition of co-crystallized X-ray structure of substrate thymidine-5′-phosphate (green) on re-docked pose (yellow) rmsd = 0.43 Å. (For interpretation of the references to color in this text, the reader is referred to the web version of the article.)

from targets and again redocked into respective receptor binding sites. The rmsd between docked pose and conformation in the crystal were determined by DSX-online tool (Fig. 2). To our delight, except two cases (*Tc*-TR and *Tc*-G3PD) the rmsd for all targets were found to be <2A° which is well within the acceptable range (see supporting material, Tables S3 and S4).

To further improve the reliability of the model, we also analyzed the clustering pattern and flexibility of the redocked molecules. Docking engine such as AutoDock is not able to manage the flexibility issues beyond a certain no. of rotational bonds (>15). Change in docking parameters and imposing restrictions in ligand flexibility can circumvent this situation to a limited extent, yet at the cost of reliability of the model. Redocked ligands with too many flexible bonds generally generate too many clusters and/or abnormal binding energies. In the absence of a suitable positive control, three proteins (*Tc*-TR, *Tc*-TS and *Mt*-MurE Ligase with 38, 24 and 31 rotational bond in co-crystallized ligand respectively) were not considered in the next stage (see supporting information, Table S4). As a result, overall four proteins were filtered out after first round of screening (Scheme 1).

Filter based on ligand efficiency/scoring function

In the absence of a common benchmark, ranking solely based on potency (here binding energy) can be biased toward a particular protein. To avoid this, an additional baseline based on ligand efficiency [38–41] was also taken into consideration which was calculated as follow:

Total binding energy of all the six co-crystallized ligands (considered as benchmark for respective proteins and screened for this round) = (−8.24) + (−6.68) + (−7.30) + (−6.42) + (−6.93) + (−8.12) = −43.69 kcal/mol
Average binding energy = −43.69/6 = −7.28 kcal/mol
Total no. of heavy atoms in 30 ligands = 613 atoms
Average no. of heavy atoms per ligand = 613/30 = 20.43 atoms
Average ligand efficiency (LE) based on the scaling of six co-crystallized ligands = −7.28/20.43 ≈ −0.35 kcal/mol per heavy atom.

This average ligand efficiency value (≈−0.35 kcal/mol per heavy atom) was quite close to consensus LE (−0.30 kcal/mol per heavy atom) proposed for fragment based lead discovery (36, 37). In the absence of common benchmark and strict cut-off, author considered higher binding affinity with good ligand efficiency (≥−0.30 kcal/mol per heavy atom) as safe criteria for defining hits. The values of ligand efficiency (LE) along with binding energy (BE) of thirty imidazo-azines are delineated in Table 2. We hoped, this would also allow a chance to all good binders to be selectively evaluated in the next step for their drug-likeness.

Following points were observed from Table 2.

a. Out of six proteins under study (in this 2nd round), *Mt*-SK showed very poor ligand efficiency (≤−0.1 kcal/mol per heavy atom). None of the ligand could cross the benchmark value in this case and hence omitted from final screening (Scheme 1).
b. Remaining five receptors *Pf*-DHFR, *Pf*-Enoyl ACPR, *Pf*-PK7, *Mt*-PS and *Mt*-TMPK produced hits with significant Ligand efficiency. Considering the inaccuracies of scoring function and absence of strict cut-off, general imidazo-azine scaffold can be safely accepted as a good binder for these proteins.
c. Amongst all imidazo-azines, six ligands from MCL019 to MCL024 showed higher LE (more negative) for all the five receptors studied. This was particularly significant for *Mt*-TMPK where the increase was about −0.10 to −0.15 kcal/mol per heavy atom. Interestingly, MCL019 to MCL024 were all unsubstituted at position 3 (R_3 = H).
d. Barrinmg one receptor *(Mt*-TMPK), two azines *namely* 2-(4-chlorophenyl)-*N*-cyclohexyl-6-methyl*H*-imidazo[1,2-*a*]pyridine-3-amine (MCL011) and *N*-cyclohexyl-2-(4-methoxyphenyl)-6-methyl*H*-imidazo[1,2-*a*]pyridine-3-amine (MCL017) exhibited maximum binding energy with accepted ligand efficiency against all the targets in question and hence were marked as "master keys" against multiple receptors (Fig. 3). Authors believe that binding of these ligands to receptor sites is mainly governed by hydrophobic interactions. Both the candidates have similar structures, except R_3 substitution. Among the set of 30 compounds, MCL011 and MCL017 have maximum molecular volume 313.149 and 325.159 Å^3 respectively, which may help them to fit well in the hydrophobic cavity. Similarly the presence of cyclohexyl group in MCL011 and MCL017 seems to render an additional stabilizing effect on the binding in *Pf*-DHFR, *Pf*-Enoyl ACPR and *Pf*-PK7. Unlike the other three receptors, it was

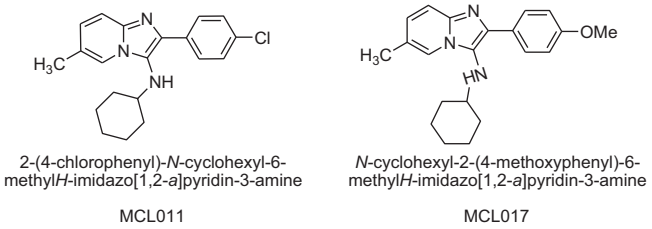

2-(4-chlorophenyl)-*N*-cyclohexyl-6-methyl*H*-imidazo[1,2-*a*]pyridin-3-amine

MCL011

N-cyclohexyl-2-(4-methoxyphenyl)-6-methyl*H*-imidazo[1,2-*a*]pyridin-3-amine

MCL017

Fig. 3. structures of the top-scorers.

Table 2
A systematic representation of docking results.

Receptors ligands	No. of heavy atoms	*Pf*-DHFR[a,b]	*Pf*-ENOYL-ACPR[a,b]	*Pf*-PK7[a,b]	*Mt*-PS[a,b]	*Mt*-TMPK[a,b]	*Mt*-SK[a,b]
MCL001	20	−0.38 (−7.55)	−0.32 (−6.34)	−0.35 (−7.09)	−0.35 (−7.02)	−0.35 (−6.80)	−0.07 (−1.51)
MCL002	21	−0.36 (−7.65)	−0.33 (−6.95)	−0.34 (−7.15)	−0.36 (−7.50)	−0.29 (−6.14)	−0.07 (−1.53)
MCL003	20	−0.36 (−7.28)	−0.30 (−6.05)	−0.34 (−6.72)	−0.33 (−6.56)	−0.27 (−5.46)	−0.07 (−1.45)
MCL004	22	−0.39 (−8.52)	−0.33 (−7.26)	−0.35 (−7.74)	−0.35 (−7.69)	−0.30 (−6.58)	−0.07 (−1.50)
MCL005	23	−0.38 (−8.83)	−0.34 (−7.76)	−0.35 (−8.07)	−0.36 (−8.26)	−0.29 (−6.57)	−0.06 (−1.52)
MCL006	22	−0.37 (−8.23)	−0.32 (−7.00)	−0.34 (−7.47)	−0.35 (−7.73)	−0.30 (−6.59)	−0.07 (−1.47)
MCL007	21	−0.40 (−8.41)	−0.34 (−7.10)	−0.35 (−7.40)	−0.35 (−7.45)	−0.30 (−6.30)	−0.07 (−1.57)
MCL008	22	−0.38 (−8.45)	−0.34 (−7.56)	−0.35 (−7.64)	−0.36 (−7.94)	−0.30 (−6.63)	−0.07 (−1.59)
MCL009	21	−0.39 (−8.15)	−0.32 (−6.69)	−0.34 (−7.08)	−0.33 (−6.99)	−0.28 (−5.98)	−0.02 (−0.34)
MCL010	23	−0.40 (−9.22)	−0.35 (−7.99)	−0.35 (−8.11)	−0.36 (−8.19)	−0.31 (−7.22)	−0.07 (−1.70)
MCL011	**24**	**−0.39 (−9.49)**	**−0.36 (−8.66)**	**−0.36 (−8.66)**	**−0.36 (−8.69)**	−0.35 (−8.39)	−0.07 (−1.72)
MCL012	23	−0.38 (−8.74)	−0.33 (−7.57)	−0.34 (−7.92)	−0.36 (−8.18)	−0.32 (−7.30)	−0.07 (−1.68)
MCL013	23	−0.35 (−8.00)	−0.29 (−6.68)	−0.34 (−7.84)	−0.31 (−7.25)	−0.27 (−6.13)	−0.06 (−1.31)
MCL014	23	−0.36 (−8.24)	−0.30 (−6.91)	−0.32 (−7.35)	−0.34 (−7.87)	−0.28 (−6.51)	−0.14 (−3.32)
MCL015	22	−0.35 (−7.71)	−0.28 (−6.17)	−0.34 (−7.46)	−0.31 (−6.80)	−0.27 (−5.93)	−0.06 (−1.24)
MCL016	24	−0.38 (−9.04)	−0.32 (−7.69)	−0.32 (−7.75)	−0.33 (−8.00)	−0.29 (−7.07)	−0.06 (−1.41)
MCL017	**25**	**−0.37 (−9.36)**	**−0.35 (−8.80)**	**−0.35 (−8.81)**	**−0.36 (−9.08)**	−0.27 (−6.77)	−0.06 (−1.44)
MCL018	24	−0.37 (−8.80)	−0.31 (−7.38)	−0.31 (−7.44)	−0.32 (−7.75)	−0.28 (−6.82)	−0.05 (−1.34)
MCL019	14	−0.40 (−5.53)	−0.40 (−5.41)	−0.40 (−5.56)	−0.38 (−5.33)	−0.40 (−5.56)	−0.09 (−1.31)
MCL020	15	−0.37 (−5.59)	−0.38 (−5.66)	−0.38 (−5.62)	−0.39 (−5.90)	−0.40 (−6.06)	−0.10 (−1.48)
MCL021	14	−0.37 (−5.14)	−0.36 (−5.02)	−0.38 (−5.28)	−0.36 (−5.11)	−0.38 (−5.29)	−0.09 (−1.26)
MCL022	16	−0.42 (−6.65)	−0.43 (−6.86)	−0.44 (−7.01)	−0.41 (−6.60)	−0.40 (−6.41)	−0.09 (−1.44)
MCL023	16	−0.42 (−6.68)	−0.45 (−7.17)	−0.42 (−6.75)	−0.46 (−7.30)	−0.43 (−6.92)	−0.09 (−1.43)
MCL024	16	−0.41 (−6.49)	−0.40 (−6.48)	−0.41 (−6.66)	−0.39 (−6.30)	−0.46 (−7.32)	−0.08 (−1.23)
MCL025	19	−0.37 (−7.10)	−0.29 (−5.48)	−0.34 (−6.48)	−0.36 (−6.83)	−0.35 (−6.69)	−0.07 (−1.35)
MCL026	20	−0.36 (−7.21)	−0.31 (−6.17)	−0.34 (−6.89)	−0.37 (−7.42)	−0.37 (−6.96)	−0.07 (−1.45)
MCL027	19	−0.36 (−6.83)	−0.27 (−5.25)	−0.31 (−5.97)	−0.33 (−6.36)	−0.31 (−5.82)	−0.07 (−1.32)
MCL028	21	−0.37 (−7.74)	−0.33 (−6.94)	−0.33 (−6.87)	−0.37 (−7.78)	−0.29 (−6.18)	−0.06 (−1.32)
MCL029	22	−0.37 (−8.10)	−0.33 (−7.33)	−0.33 (−7.19)	−0.38 (−8.31)	−0.28 (−6.21)	−0.06 (−1.35)
MCL030	21	−0.36 (−7.47)	−0.31 (−6.58)	−0.31 (−6.56)	−0.35 (−7.46)	−0.33 (−6.89)	−0.05 (−1.25)

[a] Ligand efficiency in kcal/mol/heavy atoms of 30 imidazo-azine candidates against six targets.
[b] Binding energy (in bracket) in kcal/mol. Bold values in table 2 indicate the common top scorers with acceptable ligand efficiency.

difficult to observe specific trends in *Mt*-TMPK, because of its large hydrophilic surface (Figs. 4-8, Table 3).

Consideration of lead likeness

Study like this, where medicinal spectrum of a particular scaffold is investigated, data-driven assessment of drug likeness could be a fruitful exercise. This particular concept help to identify lead/drug like hits in the initial phase of drug discovery. Since the introduction of 'Lipinski rule of five' (RO5), a more detailed analyses have been done [42]. It is generally seen that there is a significant increase in molecular weight and lipophilicity during the course of a molecule from hit to drugs. So any drug discovery process should start with even more strict criteria than employed in RO5.

From various literature reports, the following criteria have been selected for "lead-likeness" [42,43].

Molecular weight < 350 dalton
Log *P* (octanol–water) = 3–5
Maximum no. of rings < 4
Maximum no. of non terminal single bonds < 10
Maximum no. of hydrogen bond donors < 5

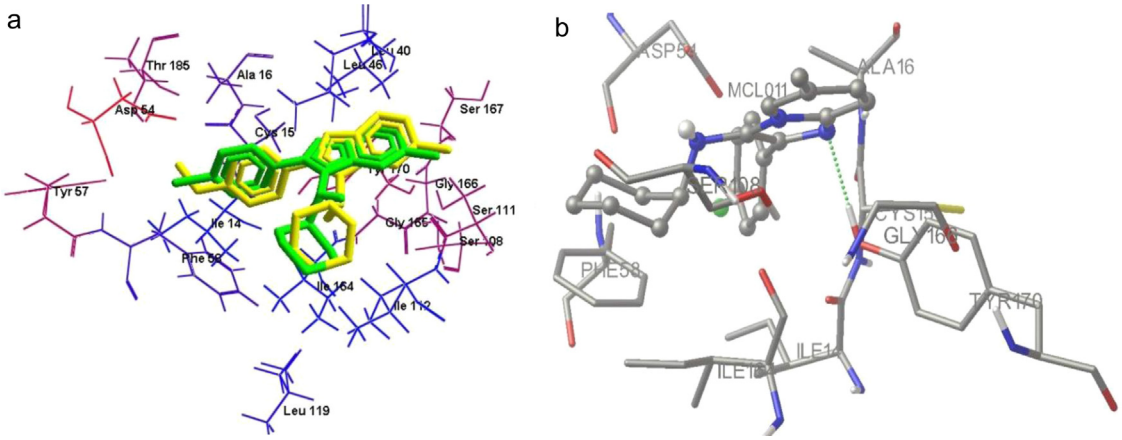

Fig. 4. (a) Binding mode of MCL011 (green) & MCL017 (yellow) surrounded by the neighboring hydrophobic (marked blue) and hydrophilic residues (marked red & pink) within 4 Å *Pf* -DHFR. (b) Hydrogen bond interaction between imidazole N-1 of MCL011 and TYR 170. (For interpretation of the references to color in this text, the reader is referred to the web version of the article.)

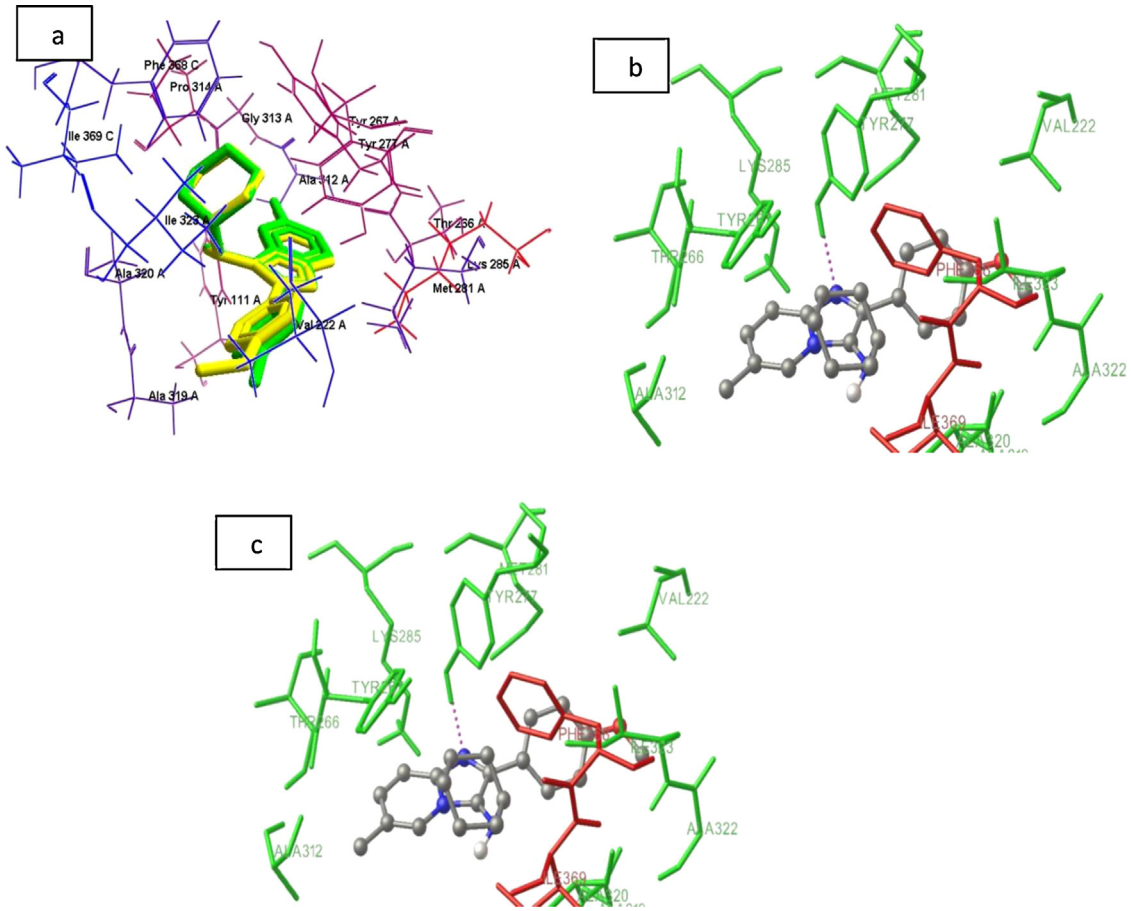

Fig. 5. (a) Binding mode of MCL011 (green) & MCL017 (yellow) surrounded by the neighboring hydrophobic (marked blue) and hydrophilic residues (marked red & pink) within 4 Å of *Pf* -Enoyl ACP Reductase. (b) Position of ligands MCL017 (c) MCL011 within the binding pocket of the *Pf*-Enoyl ACP Reductase (chain A in green, chain C in red) the hydrogen bond (dotted pink) and binding pocket is shown.

Maximum no. of hydrogen bond acceptors < 8
Ligand efficiency ≥0.30 kcal/mol/non-hydrogen atom

Keeping the above in mind' we were pleased to note that the corresponding value of descriptors for our imidazo-azine covered the following span:

Molecular weight = 190–340
Log *P* = 3–6
Maximum no. of rings = 2–4
Maximum no. of non terminal single bonds = 2–4
Maximum no. of hydrogen bond donors = 1
Maximum no. of hydrogen bond acceptors = 3–4

Table 3
Detail of binding site residues and key interactions between target and two representative imidazo-azines (MCL011 and MCL017).

Receptor	Ligand	Binding site detail (residue within 4 Å)	Hydrogen bond intraction (if any)
Pf-DHFR	MCL011	CYS 15A, ALA 16A, LEU 40A, LEU 46A, PHE 58A, ILE 112A, LEU 119A, ILE 144A, ILE 164A, TYR 170A (Fig. 4a).	N-1 imidazole moiety to TYR 170 (Fig. 4b).
	MCL017		
Pf ENOYL-ACPR	MCL011	TYR 111A, VAL 222A, TYR 277A, MET 281A, LYS 285A, ALA 312A, GLY 313A, ALA 319A, ALA 320A, ILE 323A, PHE 368 C, ILE 369A (Fig. 5a).	N-1 imidazole and TYR 277A (Fig. 5b).
	MCL017		N-1 imidazole and TYR 277A (Fig. 5c).
Pf-PK7	MCL011	LYS 55X, TYR 57X, GLU 88X, TYR 117X, GLU 118X, TYR 119X, ASP 123X, SER 176X, ASN 177X, SER 189X, ASP 190X (Fig. 6).	
	MCL017		
Mt-PS	MCL011	ASP 09A, LYS 13A, PRO 37A, TYR 39A, LEU 52A, HIS 53A, ASP 94A, ARG 95A, SER 99A, ASN 100A, ASP 163A (Fig. 7a).	
	MCL017		Methoxy oxygen and TYR 82A (Fig. 7b).
Mt-TMPK	MCL011	PRO 38A, HIS 44A, GLY 46A, HIS 47A, TYR 82A, PHE 157A, GLY 158A, LYS 160A, ASP 161A, GLN 164A, VAL 187A, MET 195A, SER 196A, SER 197 (Fig. 8a and 8b).	
	MCL017		

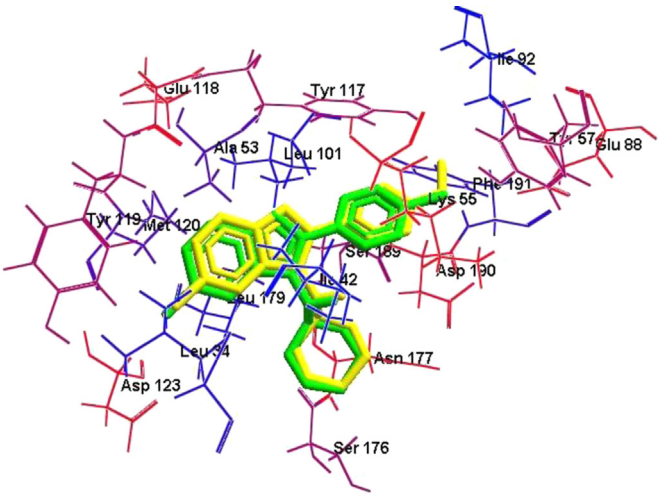

Fig. 6. MCL011 (green) & MCL017 (yellow) inside the binding pocket of *Pf*-Protein kinase 7. (Blue portion indicate hydrophobic surface while red portion show hydrophilic surface). (For interpretation of the references to color in this text, the reader is referred to the web version of the article.)

Ligand efficiency ≥−0.35 to −0.42 kcal/mol/non-hydrogen atom (*Pf*-dihydrofolate reductase)
−0.31 to −0.44 kcal/mol/non-hydrogen atom (*Pf*-enoyl acyl carrier protein reductase)
−0.28 to −0.43 kcal/mol/non-hydrogen atom (*Pf*-protein kinase 7)
−0.30 to −0.46 kcal/mol/non-hydrogen atom (*Mt*-pentothenate synthetase)
−0.27 to −0.46 kcal/mol/non-hydrogen atom (*Mt*-thymidine monophosphate)

In the absence of strict and consensus cut-off, we should accept that the computed molecular properties for our prospective azine scaffold lie well within the suggested criteria of drug/lead likeness. Features such as adequate functionality, higher potency, good ligand efficiency, optimum drug/lead likeness and easy synthetic accessibility, make this scaffold as a good starting point for future drug discovery ventures.

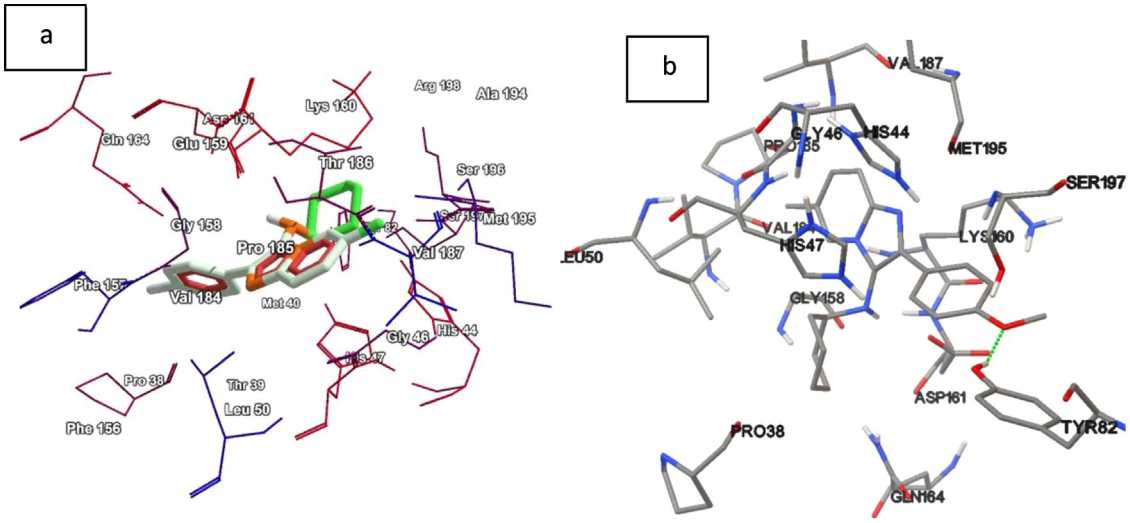

Fig. 7. (a) position of MCL011 inside the binding cavity of *Mt*-PS. Neighboring residues are colored according to their hydropathic characters. Hydrophobic residues are marked blue while hydrophilic residues are shown red. (b) Hydrogen bond interaction between ligand MCL017 and residue TYR 82.

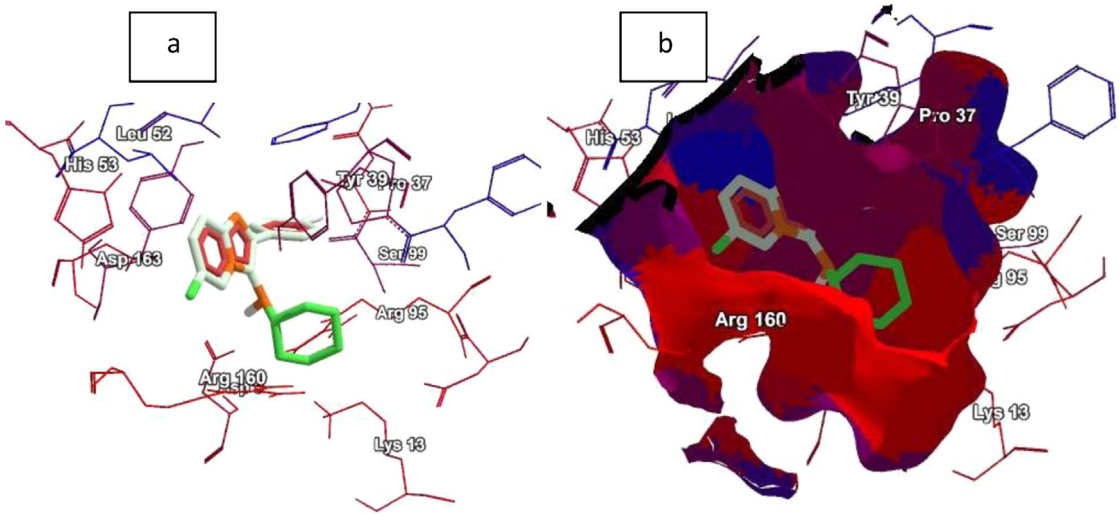

Fig. 8. (a) Neighboring residues *Mt*-TMPK surrounding MCL011. (b) Hydrophilic Surface around MCL011 (blue portion indicate.hydrophobic surface while red portion show hydrophilic surface).

Conclusion

Here a computational multitarget screening of imidazo-azines has been performed in the quest of novel inhibitors against some important tropical disease targets. Data of binding affinity and ligand efficiency suggested the chosen set of imidazo-azine scaffold as a simultaneous and selective inhibitors against multiple targets *viz*., *Pf*-dihydrofolate Reductase (DHFR), *Pf*-enoyl acyl carrier protein reductase (Enoyl ACP Reductase), *Pf*-protein kinase 7 (PK 7), *Mt*-pentothenate synthetase (*Mt*-PS) and *Mt*-thymidine monophosphate (*Mt*-TMPK). Interestingly, two compounds 2-(4-chlorophenyl)-*N*-cyclohexyl-6-methyl*H*-imidazo[1,2-*a*]pyridine-3-amine (MCL011) and *N*-cyclohexyl-2-(4-methoxyphenyl)-6-methyl*H*-imidazo[1,2-*a*]pyridine-3-amine (MCL017) have shown highest binding affinity against four targets studied (except *Mt*-TMPK) with acceptable ligand efficiency, hence can be considered as a good starting pointing.

We hope these hits might serve as an important clue toward a quest for multi-target inhibitors for the effective treatment of these diseases.

Conflict of interest

The author confirms no conflict of interest regarding the content of this article.

Acknowledgements

This work was financially supported by Department of Science and Technology (DST), Govt. of India (Grant No. SR/FT/CS-55/2011). Two of the authors B. M. and M. K. are grateful to MHRD (Govt. of India) and CSIR, Delhi for M.Tech and SRF fellowships respectively.

References

[1] F.G. de las Heras, Overview of neglected tropical diseases, Trop. Med. Chem. 7 (2011) 1–46.
[2] N.J. White, Antimalarial drug resistance, J. Clin. Invest. 113 (2004) 1084–1092.
[3] R.V. Somu, H. Boshoff, C. Qiao, E.M. Bennett, C.E. Barry, C.C. Aldrich, Rationally designed nucleoside antibiotics that inhibit siderophore biosynthesis of *Mycobacterium tuberculosis*, J. Med. Chem. 49 (2006) 31–34.
[4] G. Aguirre, E. Cabrera, H. Cerecetto, R. Di Maio, M. González, G. Seoane, A. Duffaut, A. Denicola, M.J. Gil, V. Martínez-Merino, Design, synthesis and biological evaluation of new potent 5-nitrofuryl derivatives as anti-*Trypanosoma cruzi* agents. Study of trypanothione binding site of trypanothione reductase as a target for rational design, Eur. J. Med. Chem. 39 (2004) 421–431.
[5] R.B. Lacerda, C.K.F. de Lima, L.L. da Silva, N.C. Romeiro, A.L.P. Miranda, E.J. Barreiro, C.A.M. Fraga, Discovery of novel analgesic and anti-inflammatory 3-arylamine-imidazo[1,2-a]pyridine symbiotic prototypes, Bioorg. Med. Chem. 17 (2009) 74–84.
[6] K. Zurbonsen, A. Michel, D. Vittet, P. Bonnet, C. Chevillard, Antiproliferative effects of imidazo[1,2-alpyrazine derivatives on the dami cell line, Biochem. Pharmacol. 54 (1997) 365–371.
[7] A.C. Humphries, E. Gancia, M.T.M. Gilligan, S. Goodacre, D. Hallett, K.J.S.R. Merchant, S.R. Thomas, 8-Fluoroimidazo[1,2-a]pyridine: synthesis, physicochemical properties and evaluation as a bioisosteric replacement for imidazo[1,2-a]pyrimidine in an allosteric modulator ligand of the $GABA_A$ receptor, Bioorg. Med. Chem. Lett. 16 (2006) 1518–1522.
[8] A. Gueiffier, M. Lhassani, A. Elhakmaoui, R. Snoeck, G. Andrei, O. Chavignon, J. Teulade, A. Kerbal, E.M. Essassi, J. Debouzy, M. Witvrouw, Y. Blache, J. Balzarini, E. De Clercq, J. Chapat, Synthesis of acyclo-C-nucleosides in the Imidazo[1,2-a]pyridine and pyrimidine series as antiviral agents, J. Med. Chem. 39 (1996) 2856–2859.
[9] T.H. Al-Tel, R.A. Al-Qawasmeh, R. Zaarour, Design, synthesis and in vitro antimicrobial evaluation of novel Imidazo[1,2-a]pyridine and imidazo[2,1-b][1,3]benzothiazole motifs, Eur. J. Med. Chem. 46 (2011) 1874–1881.
[10] H. Bienymé, K. Bouzid, A new heterocyclic multi-component reaction for the combinatorial synthesis of fused 3-aminoimidazole, Angew. Chem. Int. Ed. 37 (1998) 2234–2237.
[11] A. Sharma, H.-Y. Li, A regioselective and high yielding method for formaldehyde inclusion in 3CC Groebke-Blackburn-Bienymé reaction: one step access to 3-aminoimidazoazines, Synlett 10 (2011) 1407–1412.
[12] J.E. Hyde, Exploring the folate pathway in *Plasmodium falciparum*, Acta Trop. 94 (2005) 191–206.
[13] E. Jenwitheesuk, J.A. Horst, K.L. Rivas, W.C. Van Voorhis, R. Samudrala, Novel paradigms for drug discovery: computational multitarget screening, Trends Pharmacol. Sci. 29 (2008) 62–71.
[14] S. Sharma, S.K. Sharma, R. Modak, K. Karmodiya, N. Surolia, A. Surolia, Mass spectrometry-based systems approach for identification of inhibitors of *Plasmodium falciparum* fatty acid synthase, Antimicrob. Agents Chemother. 51 (2007) 2552–2558.
[15] A. Merckx, A. Echalier, K. Langford, A. Sicard, G. Langsley, J. Joore, C. Doerig, M. Noble, J. Endicott, Structures of *P. falciparum* protein kinase 7 identify an activation motif and leads for inhibitor design, Structure 16 (2008) 228–238.
[16] W.F. de Azevedo Jr., F. Canduri, J.S. de Oliveira, L.A. Basso, M.S. Palma, J.H. Pereira, D.S. Santos, Molecular model of shikimate kinase from *Mycobacterium tuberculosis*, Biochem. Biophys. Res. Commun. 295 (2002) 142–148.
[17] S. Wang, Snapshots of the Pantothenate synthetase from *Mycobacterium tuberculosis* along the reaction coordinate, Etter Trans. 1 (2005) 29–41.
[18] V. Vanheusden, H. Munier-Lehmann, M. Froeyen, R. Busson, J. Rozenski, P. Herdewijn, S.V. Calenbergh, Discovery of bicyclic thymidine analogues as selective and high-affinity inhibitors of *Mycobacterium tuberculosis* thymidine monophosphate kinase, J. Med. Chem. 47 (2004) 6187–6194.
[19] T.K. Ritter, C. Wong, Carbohydrate-based antibiotics: a new approach to tackling the problem of resistance, Angew. Chem. Int. Ed. 40 (2001) 3508–3533.
[20] C.S. Bond, Y. Zhang, M. Berriman, M.L. Cunningham, A.H. Fairlamb, W.N. Hunter, Crystal structure of *Trypanosoma cruzi* trypanothione reductase in complex with trypanothione, and the structure-based discovery of new natural product inhibitors, Structure 7 (1999) 81–89.
[21] R.V.C. Guido, G. Oliva, C.A. Montanari, A.D. Andricopulo, Structural basis for selective inhibition of trypanosomatid glyceraldehyde-3-phosphate dehydrogenase: molecular docking and 3D QSAR studies, J. Chem. Inf. Model. 48 (2008) 918–929.
[22] J. Neres, M.L. Brewer, L. Ratier, H. Botti, A. Buschiazzo, P.N. Edwards, P.N. Mortenson, M.H. Charlton, P.M. Alzari, A.C. Frasch, R.A. Bryce, K.T. Douglas, Discovery of novel inhibitors of *Trypanosoma cruzi* trans-sialidase from in silico screening, Bioorg. Med. Chem. Lett. 19 (2009) 589–596.
[23] Z. Li, H. Wan, Y. Shi, P. Ouyang, Personal experience with four kinds of chemical structure drawing software: review on ChemDraw, ChemWindow, ISIS/Draw, and ChemSketch, J. Chem. Inf. Comput. Sci. 44 (2004) 1886–1890.
[24] J. Yuvaniyama, P. Chitnumsub, S. Kamchonwongpaisan, J. Vanichtanankul, W. Sirawaraporn, P. Taylor, M.D. Walkinshaw, Y. Yuthavong, Insights into antifolate resistance from malarial DHFR-TS structures, Nat. Struct. Biol. 10 (2003) 357–365.
[25] R. Perozzo, M. Kuo, A.S. Sidhu, J.T. Valiyaveettil, R. Bittman, W.R. Jacobs Jr., D.A. Fidock, J.C. Sacchettini, Structural elucidation of the specificity of the antibacterial agent triclosan for malarial triclosan for malarial enoyl acyl carrier protein reductase, J. Biol. Chem. 277 (2002) 13106–13114.
[26] M.V. Dias, L.M. Faim, I.B. Vasconcelos, J.S. De Oliveira, L.A. Basso, D.S. Santos, W. De Azevedo, Structure of shikimate kinase from *Mycobacterium tuberculosis* complexed with ADP and shikimate at 1.9 Å of resolution, Acta Crystallogr. Sect. F 63 (2007) 1–6.
[27] S. Wang, D. Eisenberg, Crystal structures of a pantothenate synthetase from *M. tuberculosis* and its complexes with substrates and a reaction intermediate, Protein Sci. 12 (2003) 1097–1108.
[28] I. Li de la Sierra, H. Munier-Lehmann, A.M. Gilles, O. Barzu, M. Delarue, X-ray structure of TMP kinase from *Mycobacterium tuberculosis* complexed with TMP at 1.95 Å resolution, J. Mol. Biol. 311 (2001) 87–100.
[29] C. Basavannacharya, G. Robertson, T. Munshi, N.H. Keep, S. Bhakta, ATP-dependent MurE ligase in *Mycobacterium tuberculosis*: biochemical and structural characterisation, Tuberculosis 90 (2010) 16–24.
[30] S. Ladame, M.S. Castilho, C.H. Silva, C. Denier, V. Hannaert, J. Perie, G. Oliva, M. Willson, Crystal structure of *Trypanosoma cruzi* glyceraldehyde-3-phosphate dehydrogenase complexed with an analogue of 1,3-bisphospho-d-glyceric acid, Eur. J. Biochem. 270 (2003) 4574–4586.
[31] M.F. Amaya, A.G. Watts, I. Damager, A. Wehenkel, T. Nguyen, A. Buschiazzo, G. Paris, A.C. Frasch, S.G. Withers, P.M. Alzari, Structural insights into the catalytic mechanism of *Trypanosoma cruzi* trans-sialidase, Structure 12 (2004) 775–784.
[32] G.M. Morris, R. Huey, W. Lindstrom, M.F. Sanner, R.K. Belew, D.S. Goodsell, A.J. Olson, AutoDock4 and AutoDockTools4: automated docking with selective receptor flexibility, J. Comput. Chem. 30 (2009) 2785–2791.
[33] M.F. Sanner, Python: a programming language for software integration and development, J. Mol. Graph. Model. 17 (1999) 57–61.
[34] G.M. Morris, D.S. Goodsell, M.E. Pique, W.L. Lindstrom, R. Huey, S. Forli, W. Hart, S. Halliday, R.K. Belew, A.J. Olson, User guide AutoDock version 4.2, 2012, 08:37D11/P11.
[35] G. Wei, Z. Yan-Ling, A. Lu, Q. Yan-Jiang, Screening of HMG-CoA reductase inhibitors from composite salvia miltiorrhiza using Autodock, Chin. J. Nat. Med. 8 (2010) 51–56.
[36] V.C.C. Uy, J.B. Billones, Towards antituberculosis drugs: virtual screening for potential inhibitors of pantothenate synthetase of *Mycobacterium tuberculosis*, Philipp. Sci. Lett. 5 (2012) 122–130.
[37] A. Sahoo, S. Yabanoglu, B.N. Sinha, G. Ucar, A. Basu, V. Jayaprakash, Towards development of selective and reversible pyrazoline based MAO-inhibitors: synthesis, biological evaluation and docking studies, Bioorg. Med. Chem. Lett. 20 (2010) 132–136.
[38] A.L. Hopkins, C.R. Groom, A. Alex, Ligand efficiency: a useful metric for lead selection, Drug Discov. Today 9 (2004) 430–431.

[39] C. Abad-zapatero, J.T. Metz, Ligand efficiency indices as guideposts for drug discovery, Drug Discov. Today 10 (2005) 464–469.
[40] C. Abad-zapatero, Ligand efficiency indices for effective drug discovery, Expert Opin. Drug Discov. 4 (2007) 469–488.
[41] A.T. García-Sosa, S. Sild, U. Maran, Design of multi-binding site inhibitors, ligand efficiency and consensus screening of avian influenza H5N1 wild type neuraminidase and of the Oseltamivir-resistance H274Y variant, J. Chem. Inf. Model. 10 (2008) 2074–2080.
[42] M.S. Lajiness, M. Vieth, J. Erickson, Molecular properties that influence oral drug – like behaviour, Curr. Opin. Drug Discov. Devel. 7 (2004) 470–477.
[43] T. Wunberg, M. Hendrix, A. Hillisch, M. Lobell, H. Meier, C. Schmeck, H. Wild, B. Hinzen, Improving the hit-to-lead process: data-driven assessment of drug – like and lead-like screening hits, Drug Discov. Today 11 (2006) 175–180.